Draft version September 1, 2021
Preprint typeset using LaTeX style emulateapj v. 12/16/11

ANALYSIS OF THE INNER LOBES OF CENTAURUS A VIA RADIO POLARIMETRY

D. L. DePolo[1,2], C. S. Anderson[3], E. Lenc[4]

Draft version September 1, 2021

ABSTRACT

Centaurus A is a nearby, well-studied radio galaxy with history of a major merger event. The system is the nearest, radio-loud active galactic nucleus (AGN) to our galaxy, and shows a wealth of structure on all scales and wavelengths at which it has been observed. In particular, the inner and middle radio lobes present an unrivalled opportunity to study how supermassive black holes transfer energy and material to the broader cosmos. Here, we present new radio observations of the inner radio lobes, taken with the Australian Square Kilometer Array Pathfinder (ASKAP), spanning a frequency range of 747-1027 MHz and observed in full polarization. Previous work has been limited by being unable to resolve the polarization of the inner lobes of Cen A in detail over a broad frequency band. Radio polarimetry provides a means of calculating the magnetic field and determining the ratio of random to ordered components of the system. Qualitative observation of the rotation measure (RM) maps of the inner lobes reveal RM enhancement of a bow shock located in the Southwest (SW) inner lobe, previously only visible in X-ray frequencies. The RM analysis serves as a direct probe of the magnetic field strength, which we measured to be approximately 40μG. This value is substantially higher than previous estimates derived from X-ray observations, but our revised values remain too low for the shock front to act as an important source of ultra high energy cosmic rays (UHECRs). Furthermore, depolarized features within the inner lobes system are suggestive of the presence of one or more Faraday rotating regions along the line of sight to the radio source. This result has motivated the reduction and calibration of archival Jansky VLA data in order to generate a polarization spectrum spanning frequencies 0.7 - 8 GHz for the inner lobes of Cen A.

Subject headings: Galaxy Formation; Radio Galaxies; techniques: polarization

1. INTRODUCTION

Centaurus A (Cen A) is not only the brightest radio source in the Centaurus constellation, it is also our nearest powerful radio galaxy. The system itself consists of the radio source, Cen A, hosted within the giant elliptical galaxy, NGC 5128. A central dust lane through the center of NGC 5128 is evidence of a galactic merger, making the underlying physical interactions and magnetic fields of Cen A structures a well-investigated topic. See Croston et al. (2009) and Lopez-Rodriguez (2021) for examples of previous magnetic field studies at X-ray, optical, and infrared frequencies. The radio luminosity of Cen A is $L_{1.4GHz} = 2.3 \times 10^{24}$ W Hz^{-1} (Cooper et al. 1965), classifying the source as a Fanaroff-Riley class I (FRI) radio galaxy (Fanaroff & Riley 1974). The radio structure of Cen A spans far beyond the optical signatures of the galaxy; from end to end, the radio emission spans ≈ 600 kpc in the north-south direction (Neff et al. 2015a). The radio emission itself is split into four regions: the north outer lobe, the south outer lobe, the northern transition region, and the inner lobes. The inner lobes are further divided into the northeast (NE) inner lobe and the southwest (SW) inner lobe, spanning only ≈ 13 kpc between the two (Neff et al. 2015a). The radio core, associated with the AGN of NGC 5128, falls between the two inner lobes (Feain et al. 2011). The inner lobes themselves are fed by a pair of asymmetric jets, the NE and SW jets terminate in their respective inner lobes (Feain et al. 2011), refer to Figure 1a. For these reasons, Cen A provides a unique study on interactions between supermassive black holes and their environments. The close proximity of Cen A, 3.8 Mpc (Harris et al. 2010), allows for high resolution observing and subsequent detailed analysis of the system.

Polarized radio emission from the inner lobes of Cen A illuminates magnetoionic structure in the plasma surrounding the galaxy NGC 5128. This provides important astrophysical information about several key structures of astrophysical interest, including a shock system that may generate ultra-high energy cosmic rays (UHECRs; Croston et al. 2009, and the optical and molecular disk of Cen A, which encodes the history of the formation and evolution of the system (Lopez-Rodriguez 2021). We describe these more below.

Previous, multi-wavelength work has shown the inner lobes of Cen A to be a detailed and dynamic system (Israel (1998); Morganti et al. (1999); Croston et al. (2009); Eilek (2014); Neff et al. (2015b); Lopez-Rodriguez (2021)). The interactions between radio jets and surrounding gas in such regions are not fully understood, whether in Cen A (Eilek 2014), or for FRI-type sources in general. Polarimetric analysis, including Faraday rotation, may provide a powerful new probe of these regions (Guidetti et al. 2012). Deep X-ray observations reveal an edge-brightened shell surrounding the SW radio lobe (Croston et al. 2009). This structure is interpreted as a bow shock front, similar to the system seen in Cygnus A (Carilli et al. 1988). The shock has been investigated as a potential accelerating regions for ultra high energy cosmic rays (UHECRs; Croston et al. 2009). Croston et al. (2009) determined that a magnetic field strength on the order of hundreds of μG is required for the shock to efficiently accelerate UHECRs, but measured the equipartition magnetic field to be between $1-7$μG using an indirect method of estimating, based

[1] National Radio Astronomy Observatory, P. O. Box 0, Socorro, NM 87801, USA, donna.depolo@nevada.unr.edu
[2] Department of Physics, University of Nevada, Reno, NV 89557, USA
[3] Jansky Fellow of the National Radio Astronomy Observatory, P. O. Box 0, Socorro, NM 87801, USA, canderso@nrao.edu, ORCID: 0000-0002-6243-7879
[4] Astronomy and Space Science, Commonwealth Scientific and Industrial Research Organisation, P.O Box 76, Epping NSW 1710, Australia, emil.lenc@csiro.au

on their X-ray data and equipartition assumptions alone. Radio polarimetry provides a powerful, complementary, and direct estimation of the magnetic field using the physical parameters, electron density and projection along the line of sight of the magnetized region. Using radio polarimetry to calculate the magnetic field along the SW inner lobe bow shock of Cen A lends support to the conclusion reached by Croston et al. (2009).

Moreover, recent infrared (IR) and optical polarimetric observations by Lopez-Rodriguez (2021) reveal a specific pattern of magnetoionic structures in the warped molecular disk of the host galaxy NGC 5128. The authors claim these were generated by tidal forces from the previous galactic interaction, and subsequent operation of dynamos operating in NGC 5128 (Lopez-Rodriguez 2021). The inner radio jet and lobes back-illuminate parts of the warped molecular disk, but extend significantly further out, back-illuminating magnetoionic structure throughout the greater part of the host galaxy (Clarke et al. 1992). The previous study performed by Lopez-Rodriguez (2021) was limited to the infrared and optical; these wavelengths are subject to dust attenuation, leaving no emission from these wavelengths around the molecular disc to investigate the magnetic properties. The radio polarimetry data supplements and extends the magnetic field investigation from the molecular disk into the radio lobes. Sensitive polarimetric observations may therefore provide a detailed and complementary new view of the merger history and dynamics of NGC 5128.

We have undertaken a definitive broadband, full-polarization study of the inner radio lobes of Centaurus A using data from both the Australian Square Kilometre Array Pathfinder (ASKAP) and Jansky Very Large Array (VLA) radio telescopes. Our goals are to investigate the X-ray shock of the SW inner lobe, determine the magnetic field of the SW shock using radio data, compare the model from Guidetti et al. (2012), and explore the depolarization aspects of the inner lobes.

2. METHOD: BROADBAND RADIO SPECTROPOLARIMETRY

Broadband radio spectropolarimetry is a powerful means of studying magnetoionic structures of and around cosmic radio sources. Faraday rotation is an effect that probes the physical character of the magnetized plasma. The degree to which the a plane of linearly polarized light is rotated is dependent on the wavelength of light and the physical properties of the plasma. Electromagnetic radiation is emitted at a initial polarization angle (ψ_0 [rad]) and Faraday rotated to the observed polarization angle (ψ_{obs} [rad]). The observable quantity, the so-called rotation measure (RM), parametrizes the Faraday rotation and encodes information about the nature of the magnetized plasma. These quantities are related by:

$$\psi_{obs} = \psi_0 + \mathrm{RM}\lambda^2_{obs}. \tag{1}$$

By recording the RM of a target region, the magnetic field can be estimated via the following relationship (Anderson 2016):

$$RM = \frac{e^3}{2\pi m_e^2 c^4} \int_{source}^{observer} n_e \mathbf{B} \cdot d\mathbf{s} \ \mathrm{rad\ m^{-2}}, \tag{2}$$

where e is the fundamental unit of charge, m_e is the mass of an electron, c is the speed of light, n_e [cm$^-$3] is the electron density, and **s** [parsecs] is the displacement along the line of sight between the source and observer.

A simplified version of Equation 2, which assumes that the Faraday-rotating region is uniform in its properties, and takes into account the constants and units by means of a factor of proportionality, is:

$$RM = 0.812 n_e \mathbf{B} l cos(\theta), \tag{3}$$

where l is the projected distance through the region of investigation and θ is the inclination angle between the magnetic field and the line of sight. Equation 3 is used for the magnetic field calculation performed in the analysis presented in this work. From Equation 3, RM is observed and **B** [μG] can be directly calculated, with appropriate assumptions described below.

Equations 2 and 3 consider only the component of the magnetic field which is parallel to the line of sight. If the random components of the magnetic field dominate in the plasma, the RM will systematically underestimate the magnetic field strength. Fortunately, the fractional polarization provides a means of checking the ratio of random to ordered components. From Bonafede et al. (2009), the ratio can be calculated by:

$$P_{obs} = P_{intrinsic}(1 + B_r^2/B_O^2)^{-1}, \tag{4}$$

where P_{obs} is the observed polarization, $P_{intrinsic}$ is the intrinsic polarization of the source, and B_r^2/B_O^2 is the squared ratio of random to ordered components of the magnetic field. For synchrotron emitting mechanisms, such as the radio jets of Cen A, the intrinsic polarization is $\approx 70\%$.

Wavelength-dependent interference effects can also produce depolarization behaviours that provide further information about the magnetoionic structure of the system (O'Sullivan et al. 2012; Anderson et al. 2016). This provides yet another means through which sensitive, broadband radio observations can help reveal the magnetoionic structure of the plasma screen along the line of sight, back-illuminated by the radio source.

3. OBSERVATIONS, CALIBRATION, AND IMAGING

Our initial observations for this investigation came from ASKAP. Upon cursory analysis, the value of complementary high-frequency data became evident, and archival data were sought from the Jansky VLA to supplement the original observations. The ultimate goal with the data analysis is to generate a polarization spectrum of the inner lobes of Centaurus A spanning from 0.75-8 GHz. The respective observations are described in more detail below.

3.1. *ASKAP observations*

The entire Centaurus A radio lobe complex was observed using three 8-10 hour pointings of the ASKAP telescope (DeBoer et al. 2009; Johnston et al. 2007; Schinckel & Bock 2016). ASKAP consists of 36×12-m antennas, each equipped with a Phased Array Feed (PAF), yielding a $\sim$ 30 square degree instantaneous field of view. Each pointing used a `closepack36` beam footprint (McConnell et al. 2016) with a beam pitch of 0.9 degrees, covering the frequency range 747–1027 MHz (with 1 MHz channelisation). For this work, we use data from only one of these telescope pointings, which is centered on the inner lobe region (ASKAP scheduling block ID 12351).

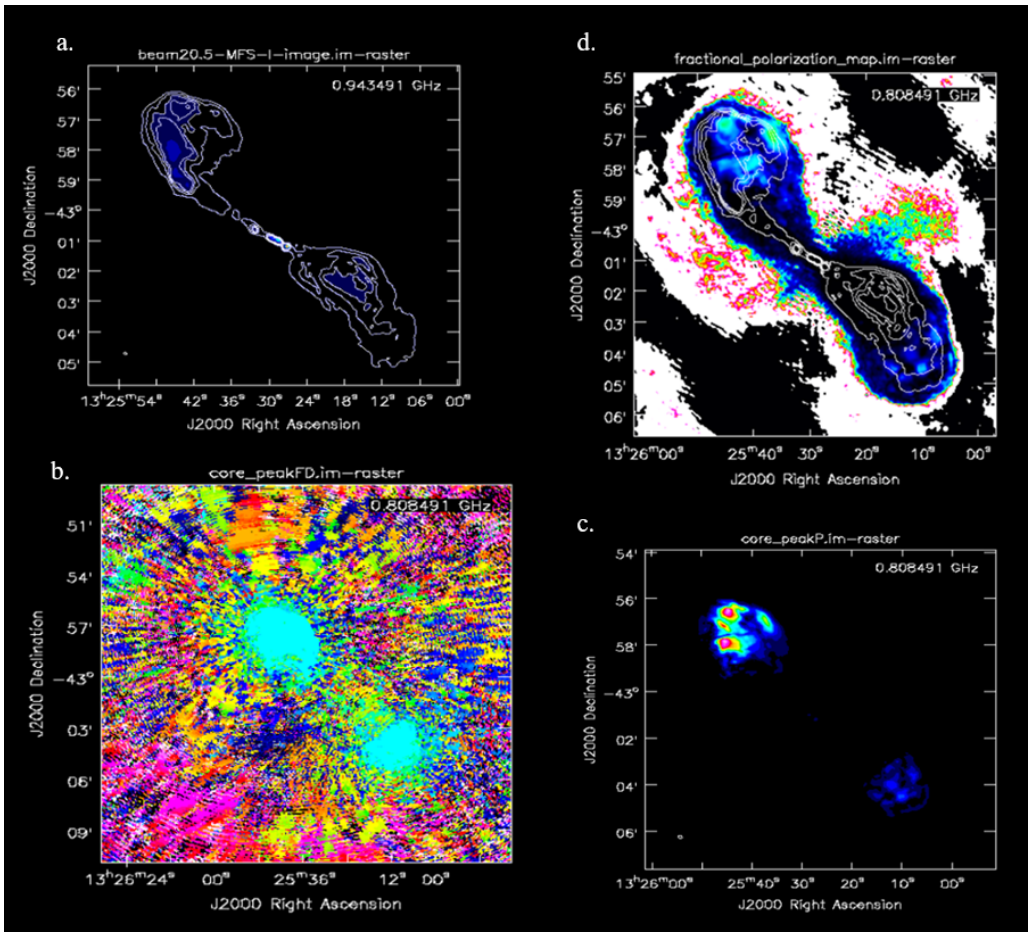

FIG. 1.— These four maps display the results of the ASKAP data. a) The stoke I map, displaying the total power of incident radiation of the inner lobes. The structures of the NE and SW inner lobes are apparent as well as the bright radio knots towards the center of the core. b) The RM map made from combining stokes Q and U data with RM synthesis. The bright orange and pink colors are background noise, while the two blue round features are the NE and SW lobes, respectively. Note the region of depolarization between the two lobes. c) The map of polarized intensity (P), $P^2 = Q^2 + U^2$. The polarized intensity also displays the dense depolarizing region between the inner lobes. d) The map of fractional polarization, made from dividing map a. from map c. The fractional polarization allows us to calculate the ratio between the random and ordered components of the magnetic field.

The data were processed in the same manner as described in Anderson et al. (2021). Briefly, we flagged and calibrated our data in the Common Astronomy Software Applications (`CASA`; McMullin et al. 2007) package. Radio frequency interference was flagged manually. We calibrated the flux scale, instrumental bandpass, and (on-axis) polarization leakage 'D-terms' using standard methods applied to observations of the (unpolarised) standard calibrator source PKS B1934–638. The instrumental XY-phase and absolute polarization angle was calibrated during beam-forming using the ASKAP on-dish calibration system (ODC; Chippendale & Anderson 2019). The off-axis polarimetric instrumental response was not corrected for this work. However, the angular extent of the target is small when compared to the full-width-half-maximum of the primary beam at our upper frequency limit $\sim$ 12 arcminutes which is about 10% of the primary beam, so the source remains squarely in the regime where on-axis polarization effects dominate. We estimate that the leakage from Stokes I to Q and U is usually less than 0.3% over the lobes (C. Anderson, private communication).

We imaged the data with `WSClean` (Offringa et al. 2014). We generated an initial multi-frequency synthesis (MFS) image of the inner lobes in total intensity with 6000 $\times$ 6000 pixels, a pixel scale of 1 arcsecond, a Briggs (1995) robust weighting value of -2 (effectively uniform weighting), local noise estimation with automatic CLEAN thresholding and masking (at 0.3 σ and 4σ respectively), and multi-scale deconvolution. We performed two rounds of self-calibration. Phase-only self-calibration was performed after the initial MFS imaging and deconvolution, and amplitude plus phase self-calibration was performed thereafter. Self-cal was performed on a per-integration basis, using only baselines longer than 200 m to avoid issues associated with missing flux from large scales in the deconvolution model.

We then re-imaged and CLEANed the Stokes I MFS map, and generated Stokes I, Q, and U datacubes with 18 MHz channelization using `WSClean`'s 'join polarizations' and 'squared channel joining' modes. The final full-band sensitivity is 115 μJy beam^{-1} per Stokes parameter. We note that this value is dynamic range limited rather than thermal noise limited due to the brightness of the inner lobes.

3.2. *Jansky VLA observations*

To augment the frequency range covered by the ASKAP observations, we are in the process of reducing and imaging archival JVLA data spanning 1-8 GHz (L, S, and C bands). The inner lobes of Centaurus A were observed on 2012 May 13 and 15 in CnB configuration, under program

code VLA/11B-117 (PI: S. Neff) [5].

In all three frequency bands, we used 3C286 for bandpass and polarization angle calibration. The source 0Q208 was used to set the amplitude scale and for the polarization leakage and phase calibration. The nearby calibrator source J1316-3338 was used to determine the complex gain solutions and phase calibration. Data were processed using standard procedures in CASA v5.6.2-3 (CASA; McMullin et al. (2007)) package.

4. RESULTS

4.1. *RM Enhancement associated with X-ray Shock*

We found that the edge-brightened bow shock in the SW inner lobe, previously only documented in the X-ray frequency, is also visible in the radio polarization and RM maps (refer to Figure 2). The ridge of polarised emission that is spatially coincident with the X-ray shock has a significance of $\approx 20\sigma$ compared to the background noise. The RM enhancement of the SW inner lobe was measured and used with Equation 3 to estimate the magnitude of the magnetic field, as detailed below.

4.2. *Magnetic Field in the Southwestern Shock System*

The RM map, Figure 2b., of the inner core of Cen A is used to measure the magnetic field along the observed SW shock front to compare with the equipotential magnetic field estimated by Croston et al. (2009). Our measurements take in account a uniform Galactic Faraday Rotation of approximately -60 rad m^{-2} (Hutschenreuter et al. 2021) across the region of investigation. More specifically, the RM enhancement associated with the shock was calculated as follows: We first subtracted a uniform RM value of -60 rad m^{-2} from the RM map to account for Galactic Faraday Rotation, then we measured the characteristic RM at the position of the shock, as well as the RM characteristic of the SW lobe, and finally we took the difference of these values. By these methods, the RM enhancement across the SW lobe is $40 \pm 0.75 radm^{-2}$.

Assuming a constant electron density of 0.004 cm^{-3} (Croston et al. 2009), a uniform magnetic field along the shock of the SW lobe, and estimating the dimensions of the lobe to be $570 \pm 50 pc$ along the line of sight (Croston et al. 2009). The magnitude of the ordered components of the magnetic field aligned along the line of sight is calculated with Equation 3:

$$\mathbf{B} = \frac{RM}{0.812 n_e l cos(\theta)} \tag{5}$$

$$= \frac{40 \pm 0.75 \mathrm{radm}^{-2}}{(0.812)(0.004 \mathrm{cm}^{-3})(570 \pm 50 \mathrm{pc}) cos(0^\circ)} \tag{6}$$

$$= 21.6 \pm 1.9 \mu G, \tag{7}$$

by setting the angle of inclination to 0° — i.e. assuming that the ordered components of the magnetic field are parallel to the line of sight to the source. This produces a minimal value for the magnitude of the magnetic field surrounding the shock cap as the calculation does not take in account magnetic reversals and non-parallel magnetic field vectors.

The polarized intensity divided by the total intensity is known as the fractional polarization. The fractional polarization, refer to Figure 1d, is the means for determining the ordered to random components of the magnetic field as it traces the geometric ordering of the magnetic field projected onto the plane of the sky (Burn 1966). We measured the characteristic fractional polarization value from the map shown in Figure 3 along the ridge of polarized emission associated with the shock. The measured fractional polarization was used with Equation 4 to determine the ratio of the random to ordered components of the magnetic field:

$$\frac{B_r^2}{B_O^2} = \frac{P_{intrinsic}}{P_{obs}} - 1 \tag{8}$$

$$\frac{B_r^2}{B_O^2} = \frac{0.70}{0.25 \pm 0.003} - 1 = 1.800 \pm 0.034 \tag{9}$$

$$\frac{B_r}{B_O} \approx 1 \tag{10}$$

To understand this calculation, it is important to note that the RM traces the ordered component of the magnetic field, parallel to the line-of-sight (l.o.s.), while the fractional polarization traces the plane-of-sky (p.o.s.), random magnetic field component. Assuming that the ordered and random magnetic field components — and by extension the l.o.s and p.o.s magnetic field components — are physically coupled, it is reasonable to estimate that $B_{\rm tot} \approx B_r + B_o$. From Equation 10, we have strengths of the random and ordered components of the magnetic field to be approximately comparable. Therefore, our previous calculation (Equation 7), which took into account the ordered components, is only about half of the total strength of the magnetic field. In order to generate an estimate of the total magnetic field strength, we then double our previous value. Thus, it is reasonable to estimate the total magnetic field strength of the SW inner lobe shock system as $B_{\rm tot} \approx B_r + B_o$, and so $B_{\rm tot}$ is $O(40)$ μG.

4.3. *Qualitative Agreement with the Guidetti Model*

Beyond the direct calculation of the magnetic field magnitude, our RM map also lends support to the generic model of radio lobe expansion into diffuse intra-group gas presented by Guidetti et al. (2012). By comparing Figures 2b & 3 (maps of RM and fractional polarization, respectively) with Figures 2c & 2d (the Guidetti model of lobe and gas geometry, and the polarimetric properties predicted therefrom, respectively), the similarities are clear. First that is, a depolarizing layer exists in the RM data map, between the NE and SW inner lobes, consistent with the depolarization indicated in the model. Additionally, the RM pattern from low to high predicted in the model is reflected in the SW inner lobe, characteristic of the bow shock. The NE inner lobe displays the moderate RM predicted in Figure 2d. Taking in account these observations, Cen A serves to support the Guidetti et al. (2012) model, which was created as a generic model to describe the jet dynamics systems within radio galaxies. Conversely, the Guidetti model may in the near future provide important insights into the distribution and magnetization of ionized gas in NGC 5128, when our analysis of supporting Jansky VLA data is complete. We describe this possibility in more detail in Section 5.

[5] Obtained from the NRAO data portal at https://data.nrao.edu/portal/

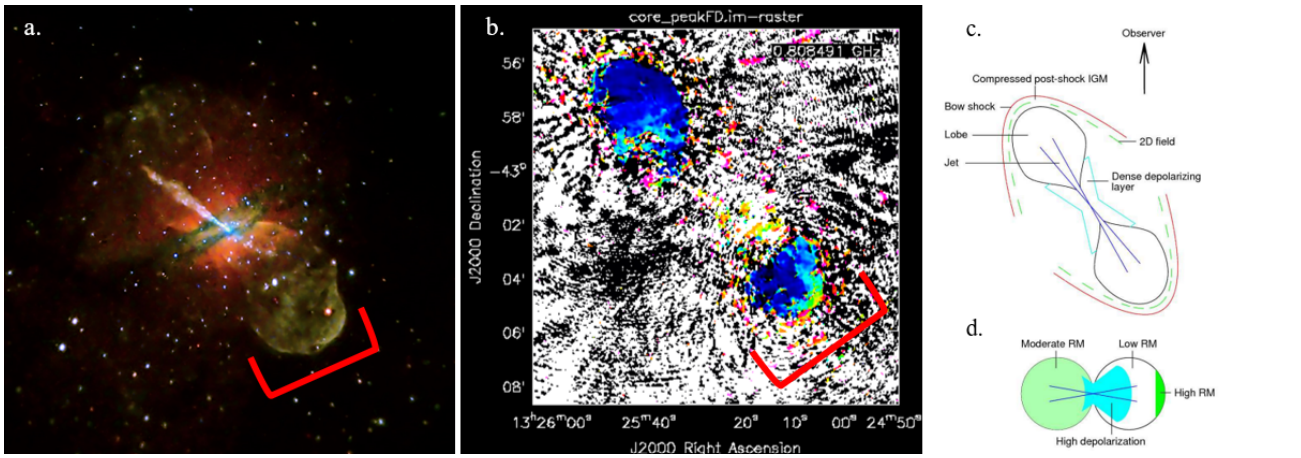

FIG. 2.— This figure emphasizes the bow shock presented in the SW inner lobe of Cen A, visible in the X-ray and the RM map. a) The X-ray image of the inner lobes, note the SW lobe bow shock, emphasized in red. b) The RM map of the inner lobes. The bow shock is visible in the SW lobe, emphasized in red and demonstrated by the RM gradient present in the figure. The black/white pattern is background noise, while the scale ranges from lower RM values (blue) to higher values (yellow). c) Generic model to describe the radio jet interaction, featuring the region of depolarization (Guidetti et al. 2012) d) Projection onto the sky of the RM model for a shock system. The RM patterns of the model are similar to the observed RM of the inner lobe system. (Guidetti et al. 2012)

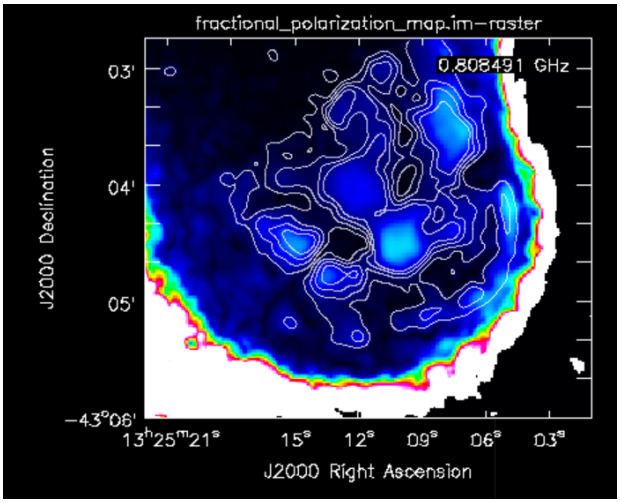

FIG. 3.— Zoom-in of the fractional polarization of the SW lobe shock. The total intensity, I, is included as the contour overlay over the fractional polarization. The fractional polarization was measured to be ≈ 25% within the bow-curved contour, closest to the terminal of the shock.

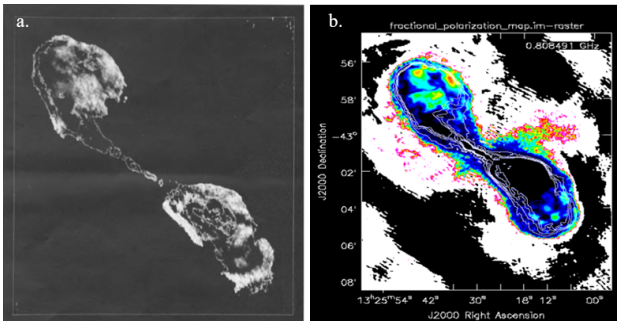

FIG. 4.— This figure compares two fractional polarization maps. a) The fractional polarization at 6 cm (5 GHz) of the inner lobes. The map scales linearly from 0 (dark) to 0.7 (light). This is a low quality polarization map from Clarke et al. (1992), however, depolarization features are notable in both the NE and SW lobes. b) The fractional polarization at 33 cm (0.9 GHz). The map scales from 0 (dark blue) to 0.7 (bright orange). There appears to be frequency dependent depolarization in the SW lobe which is indicative of Faraday rotation.

5. DISCUSSION

The X-ray brightened shock, visible in Figure 2, was originally revealed by deep observations performed by CHANDRA and analyzed by Croston et al. (2009). Croston et al. (2009) concluded that the inner lobes were an unlikely source of ultra high energy cosmic rays (UHECRs), since the magnetic field strengths they variously estimated to exist in the shock (1–7 μG, depending on methods) was at least two orders of magnitude too low to efficiently produce UHECRs. However, their methods of estimating the field strengths are based on weak equipartition arguments, or on idealised shock physics incorporating a number of untested assumptions (see their Section 4.6). Using radio polarimetry data, we can estimate the magnetic field much more directly by means of Equation 3, by which we measured a minimum magnetic field strength of $O(40)\mu$G — greater than the Croston estimate by perhaps an order of magnitude or more. Nevertheless, in order to accelerate UHECRs, a minimum magnetic field of 400μG is needed (Croston et al. 2009). To obtain a value of 400μG from Equation 6, $\theta = 87°$, nearly perpendicular. Although this is a conceivable situation, we consider it to be unlikely because a inclination of 87° (nearly the plane of the sky) orientation appears to require a specific set of conditions that lack any support of known evidence so far. Since our calculation is an order of magnitude below the minimum cutoff for accelerating UHECRs, we tentatively agree with Croston et al. (2009)'s conclusion that the inner lobes of Cen A remain an unlikely source of UHECRs.

The depolarization effects seen in Figure 4 appear to be dependent on frequency. The fractional polarization structure of the NE lobe is similar between the Clarke1992 map and the ASKAP map. However, the emission in the 0.9 GHz SW lobe is depolarized, while there is polarized emission visible in the lower resolution 5 GHz map. This may be indicative of a turbulent Faraday rotating screen along the line of sight, between the observer and the radio emitter. Future work on our archival Jansky VLA data will examine this possibility. Currently, our ASKAP data effectively comprise a single snapshot of the polarization spectrum of the inner lobes at a specific frequency. The broadband Jansky VLA data adds substantial new information to elucidate the physical properties of magnetised plasma near the source, in a manner directly

analogous to how adding baselines of different lengths to an aperture synthesis telescope helps elucidate the spatial structure of radio sources. When the data are fully calibrated, we will analyze the data using cutting-edge techniques such as *qu*-fitting (Anderson et al. 2016) as well as RM synthesis.

Beyond our stated results, several features of the ASKAP data we imaged are interesting for future works. The depolarization features of the NE and SW lobes has motivated future investigations into archival Jansky VLA data. As previously mentioned, the VLA data reduction and imaging are currently being performed to complete RM synthesis and QU-fitting analysis. The goal is to generate a polarization spectrum spanning from 0.8-8 GHz. The cursory investigation will consist of fractional polarization maps, similar to Figure 4, constructed side-by-side with similar resolution. We will qualitatively be looking for polarized emission present in the depolarized regions of the SW lobe in higher frequencies. These results will either confirm or deny the existence of a Faraday rotation screen located, along the line of sight, in front of the SW inner lobe.

Another notable feature of the inner lobes is visible in Figure 5. Figure 5 is the same image as Figure 1a, with different scaling. Once the bright emission of the inner core is scaled to look deeper into the background, a faint, twisted disk begins to appear perpendicular to the radio lobes. This faint radio emission is coincident with the molecular disk, visible in the optical. Not only is this feature visible in the total intensity map, a disk-like feature is suggested in the Figure 1d, the fractional polarization. Therefore future investigation will look into the significance and magnetic properties of the disk-like signal. This particular investigation of the magnetic fields of molecular disk extended into the radio lobes using radio polarimetry will supplement the work performed by Lopez-Rodriguez (2021).

The final distinct region in our data is the North Transition Region. The large region located north of the inner lobes, refer to Figure 6. The north transition region is of particular interest in the Cen A system, as the energy flow mechanism of the region is still not fully understood. Some models have attempted to explain the dynamics of the observed data, including buoyant, magnetic tower, and flow-driven models (Eilek 2014). These models need to be developed further before being tested against the observational data. Neff et al. (2015b) suggest a galactic wind is driving the dynamics and weather seen in the North Transition Region. More research into RM structures and our data could provide evidence to support or refute the galactic wind theory. Future studies in this region may include collaboration with another research group, depending on data quality and analysis progress.

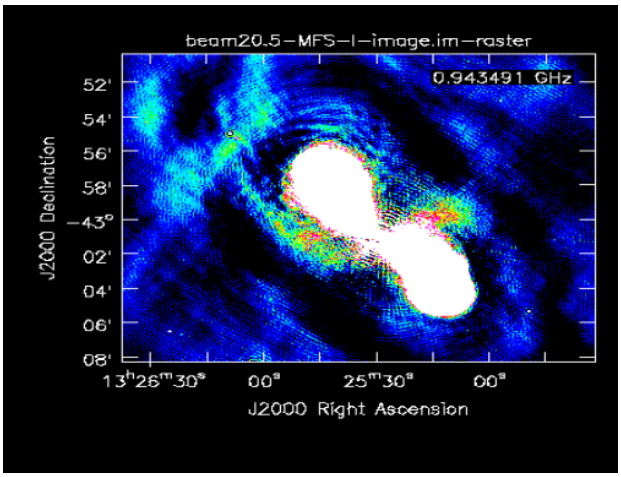

FIG. 5.— Total intensity map of the inner lobes centered at 0.94 GHz. The scaling of this image was shifted so that the faint radio emission, oragne/green regions perpendicular to the radio lobes, is visible over the bright, white, radio lobes. This faint, disk-like emission is coincident with the optical molecular disk of NGC 5128.

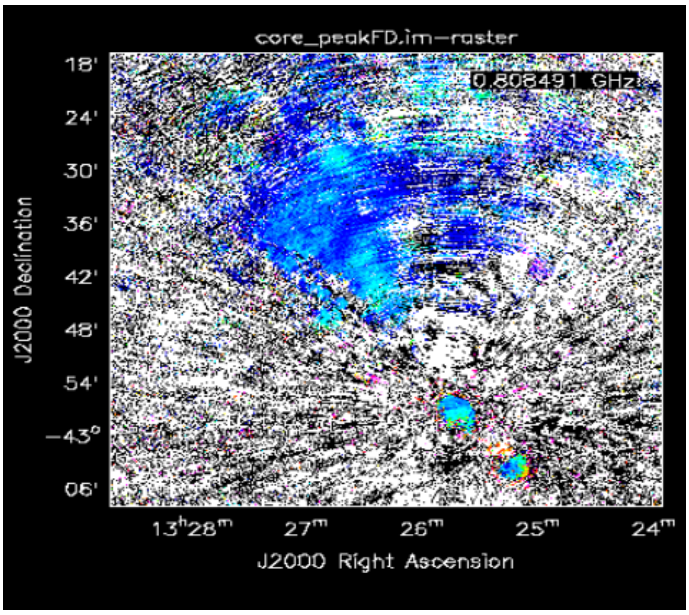

FIG. 6.— Zoom-out of the RM map. Visible is the bottom right are the two inner lobes. North of the inner lobes is a wide swath of blue indicating the north transition region of Cen A. The energy flow mechanisms of the north transition region are poorly understood, however, the RM map might provide clues into the radio and magnetic structure of this part of the radio galaxy.

6. SUMMARY AND CONCLUSIONS

We studied the inner lobes of Cen A using ASKAP in from 747 - 1027 MHz, using RM synthesis to create maps to measure the RM in order to calculate the magnitude of the magnetic field along the SW radio lobe shock. We measured a value $O(40)\mu$G, which is at least an order of magnitude higher than previous estimates, but still ultimately supports previous conclusions that the region is probably not important for accelerating UHECRs. In addition, our RM map of the inner lobes is strikingly consistent with the generic Guidetti et al. (2012) model describing the interaction of expanding radio lobes with diffuse intra-group gas, and the predicted RM and polarimetric signatures of this gas in a radio jet dynamic region.

In ongoing work, we intend to complete our calibration of Jansky VLA data from 1–8 GHz. We will then exploit the combined ASKAP and Jansky VLA data sets as an exquisite probe of distribution, structure and magnetisation of gas in the SW inner lobe, along the warped disk, and through the North Transition Region structures discussed in Section 5. We expect this will also shed new light on the flow of energy through the Cen A system, and how the supermassive black hole in NGC 5128 interacts with its host galaxy and beyond. Since Cen A is the prototypical FRI-type radio galaxy, our work will set the stage for future, deeper observations of statistical samples of more distant FRI radio galaxies with the ngVLA and beyond.

D.L. deP. would like to thank the National Radio Astronomy Observatory for funding and the opportunity to perform this research. Specifically thanking A. Kapinska, J. Braatz, and W. Armentrout for their mentorship during this project. C. S. A. is a Jansky Fellow of the National Radio Astronomy Observatory. This work employed ASKAP data from scheduling block 12351. The Australian SKA Pathfinder is part of the Australia Telescope National Facility which is managed by CSIRO. Operation of ASKAP is funded by the Australian Government with support from the National Collaborative Research Infrastructure Strategy. ASKAP uses the resources of the Pawsey Supercomputing centre. Establishment of ASKAP, the Murchison Radio-astronomy Observatory and the Pawsey Supercomputing Centre are initiatives of the Australian Government, with support from the Government of Western Australia and the Science and Industry Endowment Fund. We acknowledge the Wajarri Yamatji people as the traditional owners of the Observatory site. This work employed VLA data from project 11B-117. The National Radio Astronomy Observatory is a facility of the National Science Foundation operated under cooperative agreement by Associated Universities, Inc.

REFERENCES

Anderson C., 2016, PhD thesis, The University of Sydney
Anderson C. S., Gaensler B. M., Feain I. J., 2016, ApJ, 825, 59
Anderson C. S., et al., 2021, , 38, e020
Bonafede A., et al., 2009, A&A, 503, 707
Briggs D. S., 1995, in American Astronomical Society Meeting Abstracts. p. 1444
Burn B. J., 1966, MNRAS, 133, 67
Carilli C. L., Perley R. A., Dreher J. H., 1988, ApJ, 334, L73
Chippendale A., Anderson C., 2019, 019, On-Dish Calibration of XY Phase for ASKAP's Phased Array Feeds, https://www.atnf.csiro.au/projects/askap/ACES-memos. Commonwealth Scientific and Industrial Research Organisation, https://www.atnf.csiro.au/projects/askap/ACES-memos
Clarke D. A., Bridle A. H., Burns J. O., Perley R. A., Norman M. L., 1992, ApJ, 385, 173
Cooper B., Price R., Cole D., 1965, Australian Journal of Physics, 18, 590
Croston J. H., et al., 2009, MNRAS, 395, 1999
DeBoer D. R., et al., 2009, IEEE Proceedings, 97, 1507
Eilek J. A., 2014, New Journal of Physics, 16, 045001
Fanaroff B. L., Riley J. M., 1974, MNRAS, 167, 31P
Feain I. J., et al., 2011, ApJ, 740, 17
Guidetti D., Laing R. A., Croston J. H., Bridle A. H., Parma P., 2012, MNRAS, 423, 1335
Harris G. L. H., Rejkuba M., Harris W. E., 2010, , 27, 457
Hutschenreuter S., et al., 2021, arXiv e-prints, p. arXiv:2102.01709
Israel F. P., 1998, A&A Rev., 8, 237
Johnston S., et al., 2007, , 24, 174
Lopez-Rodriguez E., 2021, Nature Astronomy, 5, 604
McConnell D., et al., 2016, , 33, e042
McMullin J. P., Waters B., Schiebel D., Young W., Golap K., 2007, CASA Architecture and Applications. p. 127
Morganti R., Killeen N. E. B., Ekers R. D., Oosterloo T. A., 1999, MNRAS, 307, 750
Neff S. G., Eilek J. A., Owen F. N., 2015a, ApJ, 802, 87
Neff S. G., Eilek J. A., Owen F. N., 2015b, ApJ, 802, 88
O'Sullivan S. P., et al., 2012, MNRAS, 421, 3300
Offringa A. R., McKinley B., Hurley-Walker et al., 2014, MNRAS, 444, 606
Schinckel A. E. T., Bock D. C.-J., 2016, in Proc. SPIE Ground-based and Airborne Telescopes VI. p. 99062A, doi:10.1117/12.2233920